

# Thermodynamic and Structural Studies of Cavity Formation in Proteins Suggest That Loss of Packing Interactions Rather Than the Hydrophobic Effect Dominates the Observed Energetics<sup>†,‡</sup>

Girish S. Ratnaparkhi<sup>§,||</sup> and R. Varadarajan<sup>\*,§,⊥</sup>

Molecular Biophysics Unit, Indian Institute of Science, Bangalore 560 012, India, National Centre for Biological Sciences, TIFR Centre, Bangalore 560065, India, and Chemical Biology Unit, Jawaharlal Nehru Center for Advanced Scientific Research, Jakkur P.O., Bangalore 560 064, India

Received April 5, 2000; Revised Manuscript Received July 5, 2000

**ABSTRACT:** The hydrophobic effect is widely believed to be an important determinant of protein stability. However, it is difficult to obtain unambiguous experimental estimates of the contribution of the hydrophobic driving force to the overall free energy of folding. Thermodynamic and structural studies of large to small substitutions in proteins are the most direct method of measuring this contribution. We have substituted the buried residue Phe8 in RNase S with alanine, methionine, and norleucine. Binding thermodynamics and structures were characterized by titration calorimetry and crystallography, respectively. The crystal structures of the RNase S F8A, F8M, and F8Nle mutants indicate that the protein tolerates the changes without any main chain adjustments. The correlation of structural and thermodynamic parameters associated with large to small substitutions was analyzed for nine mutants of RNase S as well as 32 additional cavity-containing mutants of T4 lysozyme, human lysozyme, and barnase. Such substitutions were typically found to result in negligible changes in  $\Delta C_p$  and positive values of both  $\Delta\Delta H^\circ$  and  $\Delta\Delta S^\circ$  of folding. Enthalpic effects were dominant, and the sign of  $\Delta\Delta S^\circ$  is the opposite of that expected from the hydrophobic effect. Values of  $\Delta\Delta G^\circ$  and  $\Delta\Delta H^\circ$  correlated better with changes in packing parameters such as residue depth or occluded surface than with the change in accessible surface area upon folding. These results suggest that the loss of packing interactions rather than the hydrophobic effect is a dominant contributor to the observed energetics for large to small substitutions. Hence, estimates of the magnitude of the hydrophobic driving force derived from earlier mutational studies are likely to be significantly in excess of the actual value.

It is generally thought that most folded protein structures observed in nature lie at a global minimum in free energy. While the various interactions that stabilize a protein relative to its unfolded state have been qualitatively understood for some time, a quantitative understanding remains elusive. Monomeric, globular proteins typically have free energies of folding ( $\Delta G^\circ_f$ ) in the range of  $-5$  to  $-15$  kcal/mol. The hydrophobic driving force ( $1-4$ ) is widely believed to be one of the most important determinants of protein stability. This belief is based to a large degree on the observation that nonpolar molecules have favorable, negative free energies of transfer ( $\Delta G^\circ_{tr}$ ) from water to organic solvents. At room temperature, nonpolar, aliphatic chains have positive enthal-

pies ( $\Delta H^\circ_{tr}$ ) and entropies ( $\Delta S_{tr}$ ) and negative heat capacities ( $\Delta C_{ptr}$ ) of transfer ( $1, 3, 5$ ). The absolute magnitudes of all four quantities increase with increases in nonpolar surface area. At room temperature, the entropic component is dominant, though at high temperatures the transfer process is enthalpy-driven ( $6, 7$ ). The positive value of  $\Delta S_{tr}$  is thought to arise from ordering of water molecules around the nonpolar solute. When the protein folds, several nonpolar side chains that are exposed in the unfolded state become inaccessible to solvent. The unfavorable entropy associated with hydration of these nonpolar side chains in the unfolded state is thought to be one of the driving forces for protein folding. The hydrophobic driving force is typically quantitated in terms of the nonpolar surface area buried upon folding. It is difficult to obtain direct experimental estimates of the contribution of the hydrophobic driving force to the measured value of  $\Delta G^\circ_f$ . In protein folding, this is because there are many contributions to  $\Delta G^\circ_f$ . These include differences in hydrogen bonding, van der Waals interactions, electrostatics, and conformational entropy between the folded and unfolded states. Protein engineering studies offer a potential solution to this problem. Mutation of large, buried, nonpolar residues to smaller nonpolar ones will result in a decreased hydrophobic driving force for folding which

<sup>†</sup> This work was supported by grants from DST and DBT, Government of India, to R.V.

<sup>‡</sup> The coordinates and structure factors of the F8A, F8Met, and F8Nle mutants have been deposited and released by the Research Collaboratory for Structural Bioinformatics (RCSB) as Protein Data Bank entries 1D5H, 1D5D, and 1D5E, respectively.

\* To whom correspondence should be addressed: Molecular Biophysics Unit, Indian Institute of Science, Bangalore 560 012, India. E-mail: varadar@mbu.iisc.ernet.in. Phone: 011-91-80-3092612. Fax: 011-91-80-3600535, 91-80-3600683.

<sup>§</sup> Indian Institute of Science.

<sup>||</sup> National Centre for Biological Sciences.

<sup>⊥</sup> Jawaharlal Nehru Center for Advanced Scientific Research.

Table 1: Summary of Data Collection, Reduction, and Refinement for the Residue 8 Mutants of RNase S

mutant (PDB ID)	$a = b$ (Å)	$c$ (Å)	$R_{\text{merge}}^a$ (%)	no. of unique <sup>b</sup> reflections	resolution <sup>c</sup>	no. of waters	$R$	$R_{\text{free}}$	rms deviation	
									bond lengths (Å)	bond angles (deg)
F8A (1D5H)	44.71	97.52	6.0	5238	2.25	35	21.0	25.7	0.012	1.6
F8M (1D5D)	44.84	98.00	11.7	4492	2.25	46	18.9	21.8	0.005	1.3
F8Nle (1D5E)	44.60	98.07	9.6	4923	2.25	46	20.9	23.1	0.006	1.6

<sup>a</sup>  $R_{\text{merge}} = 100 \times \sum |I_h - \langle I \rangle| / \sum I_h$ , where  $I_h$  is the intensity of reflection  $h$ . <sup>b</sup> Number of unique, non-zero reflections used for refinement. <sup>c</sup> The shell at which >50% (>2 $\sigma$ ) of the expected reflections are present.

can be correlated with the difference in  $\Delta G^\circ_f$  [ $\Delta\Delta G^\circ_f = \Delta G^\circ_f(\text{mutant}) - \Delta G^\circ_f(\text{wild type})$ ] upon mutation. Early studies of such mutational effects (8–10) showed a linear correlation between values of  $\Delta\Delta G^\circ_f$  and  $\Delta\Delta G^\circ_{\text{tr}}$ , suggesting that the effect of the mutation on stability is indeed primarily due to changes in the hydrophobic driving force. An implicit assumption here is that the structures of wild type and mutant proteins are identical. Subsequent studies (11–15) showed that in several cases, large to small substitutions are accompanied by cavity formation at the site of substitution. Hence, in addition to the hydrophobic effect, loss of van der Waals interactions in the mutant structure will also contribute to the observed energetics. In the work presented here, we show that this latter effect is likely to be the dominant contributor and that the observed sign of  $\Delta\Delta S_f$  is the opposite of that expected from the hydrophobic effect. Furthermore, the mutational studies show that stability decreases are always due to positive values of  $\Delta\Delta H$  (enthalpy-dominated). In contrast, for small molecule transfer studies, the observed thermodynamics is generally entropy-dominated.

The experimental system consists of the protein–peptide complex ribonuclease S (RNase S).<sup>1</sup> This is obtained by cleavage of bovine pancreatic ribonuclease A (RNase A) with subtilisin to give two fragments, S peptide (residues 1–20) and S protein (residues 21–124) (16, 17). These fragments can be reconstituted to give the catalytically active complex RNase S, having a structure very similar to that of RNase A (18). As residues 16–20 are not important for binding to the S protein, we use a truncated version of the S peptide consisting of the first 15 residues with a C-terminal amide designated S15. Two hydrophobic residues, methionine 13 (M13) and phenylalanine 8 (F8), of the S peptide contribute significantly to the stability of RNase S. Both residues are buried inside the core of RNase S, burying accessible nonpolar surface areas of 67 and 115 Å<sup>2</sup>, respectively. F8 is a critical residue for the stability of RNase S (17) and makes an important contribution to the energetics of the transition state during folding (19).

In earlier studies, eight hydrophobic residues ranging in size from Gly to Phe were substituted at position 13 in S15. The structures of these S15 mutant complexes with the S protein were studied using X-ray crystallography (13, 20).

<sup>1</sup> Abbreviations: RNase A, bovine pancreatic ribonuclease; RNase S, product of proteolytic cleavage of the bond between positions 20 and 21 in RNase A; Nle, norleucine; S15, 15-residue S peptide with the amino acid sequence KETAAAKFERQHMDS, with the C-terminus amidated; F8X, replacement of Phe8 with side chain X, where X is Ala (A), Met (M), or Nle; M13X, replacement of the Met13 side chain with side chain X; OS, occluded surface; ASA, accessible surface area; MC, main chain; SC, side chain; RMSD, root-mean-square deviation; ANB,  $\alpha$ -aminobutyric acid.

The free energies ( $\Delta G^\circ$ ), enthalpies ( $\Delta H^\circ$ ), and entropies ( $\Delta S$ ) (21) and the heat capacities ( $\Delta C_p$ ) (20, 22) of the binding of these substituted analogues to the S protein were measured using titration calorimetry. A unique feature of the RNase S system is that it is possible to study mutational effects on thermodynamic parameters at room temperature in the absence of denaturants (21). Furthermore, values of  $\Delta C_p$  measured using titration calorimetry in the RNase S system are more accurate than values obtained using DSC, and it is possible to examine mutational effects on  $\Delta C_p$ . In this study, we have substituted F8 with three smaller hydrophobic residues, methionine (M), norleucine (Nle), and alanine (A). The replacements of F8 with Met and Nle were undertaken because of the unusually large changes in  $\Delta H^\circ$  and  $\Delta S$  previously observed for the M13Nle substitution. The two chains differ only by the replacement of a sulfur atom with a less polar methylene group (20). The replacement of the bulky Phe residue with smaller residues also allows us to study effects of nondisruptive mutations in RNase S. In addition, the energetics of cavity formation in a set of 38 additional cavity creating mutations in RNase S, T4 lysozyme, human lysozyme, and barnase were analyzed. All the data support the thesis that the loss of packing interactions rather than the hydrophobic effect dominates the observed energetics.

## MATERIALS AND METHODS

**Materials.** RNase A (type XII A), subtilisin Carlsberg, and ammonium sulfate were purchased from Sigma Chemical Co. RNase S and S protein were prepared and purified as described previously (23). The F8M, F8Nle, and F8A are 15-residue peptides that have amidated C-termini. S(4–14) and S(8–14) are deletion peptides with free C-termini, and acetylated N-termini, containing only residues 4–14 and 8–14 of the sequence of the S15(M13L) peptide, respectively.

**Crystallization and Titration Calorimetry.** Crystallization and titration calorimetry for the F8M, F8Nle, and F8A was carried out as described previously (13, 20–22). Data collection, reduction, and refinement were carried out as described previously (24). Table 1 lists the three crystallographic data sets collected, while the titration calorimetric data (in the temperature range of 6–25 °C) for the three mutants are available as Supporting Information.

**Analysis.** Parameters such as accessible surface area (ASA; 25, 26), depth (27), and occluded surface (OS; 28) were examined. Occluded surface is defined as the molecular surface that is less than 2.8 Å from the van der Waals surface of neighboring, but nonbonded atoms. The OS is very sensitive to changes in packing geometry. The OS is calculated for each residue of the protein by summing up

OS values of individual atoms. The  $\Delta\text{OS}$  ( $\Delta\text{OS} = \Sigma\text{OS}_{\text{mut}} - \Sigma\text{OS}_{\text{wt}}$ ) was calculated for each structure.  $\Sigma\text{OS}$  is the sum of the OS for residues within 4 Å of any atom of the replaced residue (including the OS of the replaced residue). The change in depth ( $\Delta\text{Depth}$ ) of the side chain between the mutant and wild type residue, summed over all the side chains atoms for that residue, was also used for analysis (27). The  $\Delta\Delta\text{ASA}$  (26) was calculated for all 45 structures as described previously (27).

The program VOIDOO (29) was used to analyze cavities in RNase S mutant structures with a 1.2 Å probe. The parameters chosen gave cavity volumes for the M13X mutants similar to those calculated previously using a Voronoi procedure (13). Different orientations of the RNase S molecule were used, and the average volumes from these calculations were taken as the volume of the cavity. The errors in calculation were approximately 10–20% of the cavity volume.

The OS, depth, and cavity volumes were also calculated for all cavity-containing mutants of T4 lysozyme (12, 30), human lysozyme (31, 32), and barnase (33), where single, nondisruptive, mutations of large to small hydrophobic residues have been introduced. The cavity volumes for RNase S mutants and these additional mutant structures were calculated using the Molecular surface package (MSP; 25) and a 1.2 Å probe so that the results would be consistent with previously published work. The cavity volume was set to zero if no cavity was detected using this probe radius. The PDB codes (34) of the deposited coordinates are 1rny, 1rbc, 1rbd, 1rbf, 1rbg, 1rbh, 1rbi, 2rln, 1d5d, 1d5e, and 1d5h for RNase S, 1163, 1167, 1169, 1185, 1190, 2001, 2351, 2361, 2381, 2401, 2431, and 2441 for L118A T4 lysozyme, 11z1, 1yam, 1yan, 1yao, 1yap, 1yaa, 1oub, 1ouc, 1oud, 1oue, 1ouf, 1oug, 1ouh, 1oui, and 1ouj for human lysozyme, and 1bni, 1brh, 1bri, 1brj, 1brk, and 1bse for barnase. In each case, the wild type structure has been underlined. The structural parameters determined for these 41 mutants were correlated with thermodynamic data for folding or binding.

The thermodynamic parameters for RNase S have been measured using titration calorimetry and are from ref 20 and this work. The thermodynamic parameters and the errors in these parameters for T4 lysozyme (12, 30), human lysozyme (31, 32), and barnase (33, 35) were taken from published data. The thermal unfolding of both human lysozyme and barnase has been shown to be two-state using differential scanning calorimetry (DSC) (31–33, 35). The data for T4 lysozyme (12, 30) have been obtained by van't Hoff formalism, and we have an estimate of the errors associated with  $\Delta G^\circ$  only. The correction for the “hydrophobic” component of the  $\Delta G^\circ_{\text{obs}}$  was derived by subtracting the  $\Delta G^\circ_{\text{tr}}$  for the mutant amino acid ( $\Delta\Delta G^\circ_{\text{corr}} = \Delta\Delta G^\circ_{\text{obs}} - \Delta\Delta G^\circ_{\text{tr}}$ ), on the basis of the hydrophobicity scale of Fauchere and Pliska (36). This scale is based on the transfer of amino acids from water to *n*-octanol at 25 °C. The  $\Delta G^\circ_{\text{tr}}$  values for Nle and  $\alpha$ -aminobutyric acid (ANB) used in this study are from ref 37. The convention of  $\Delta\Delta X = \Delta X_{\text{mutant}} - \Delta X_{\text{wild type}}$ , where  $X$  is  $G^\circ$ ,  $H^\circ$ ,  $C_p$ , OS, depth, or ASA, has been followed throughout.

## RESULTS

*Structural Changes in the RNase S (F8X) Mutants.* Mutant structures were compared to each other and to their respective

controls. The F8M, F8A, and F8Nle structures were similar to each other in their overall structure. The only side chain exhibiting a significant change was F120 in the F8A structure. The replacement of the wt Phe with Ala, Met, or Nle should cause the formation of a 112, 33, or 33 Å<sup>3</sup> cavity (Voronoi volumes), respectively. A single 15, 9, or 7 Å<sup>3</sup> cavity was found in the structures in the region near the mutation site in the respective mutant. The cavity in the F8A mutant was much smaller than expected for a Phe → Ala substitution because of the movement of F120 into the potential cavity. Figure 1 displays the cavities detected in the F8A and F8Met structures by displaying the dot surfaces of the residues surrounding the mutation site. A model of the F8A mutant (Figure 1A) shows that the replacement of F8 with Ala should create a cavity within the protein. The actual structure of the F8A mutant shows that the potential cavity is minimized by the movement of the F120 side chain into the cavity (Figure 1B). The structures of the F8M and F8Nle mutants are similar, and the small cavity created is tolerated without any changes in the structure (Figure 1C). The side chains of M8 (−163°, 84°, and 169°) and Nle8 (−150°, 100°, and 178°) also have similar conformations, and for this reason, only one of the structures is shown (F8M, Figure 1C). The F120 side chain is not perturbed in either the F8M or F8Nle structure (Figure 1C). In the F8A structure, the F120 side chain undergoes a  $\chi_1$  change (by 80°) toward the potential cavity created by the F8A mutation. The side chains of the Ala, Met, and Nle residues at position 8 as well as F120 in the F8A structure exhibit  $\chi_1$  values near gauche or anti conformations. The  $\Delta B$ -factor plots ( $B_{\text{F8X}} - B_{\text{control}}$ ) for the F8M and F8Nle mutants indicated (data not shown) that the residues in van der Waals contact (4 Å) with the mutation site were not perturbed significantly.

VOIDOO (29) could not detect any cavity in the original (wt) space occupied by the F120 side chain in the F8A structure. This may be because of the proximity of this cavity to the surface. The changes in packing due to mutation were quantitated in terms of changes in the OS parameter (28). The side chain of F120 had similar OS values (79.9, 77.1, 77.9, and 81.6 Å<sup>2</sup> for F8A, F8M, F8Nle, and wt, respectively) in all three mutant structures and in the controls, indicating that the movement of the F120 side chain in the F8A structure did not affect its packing with its neighbors. Most water molecules did not differ significantly in terms of their position or  $B$ -factors compared to their respective controls. No ordered water molecules were observed in any of the cavities. Modeling studies showed that it was possible to accommodate a water at only a single location in the cavity without severe steric overlap in F8A. In no case were there any appropriately placed hydrogen bond donors or acceptors. Since the sterically allowed volume for a putative water in the cavity around residue 8 is small, any water present would have to be ordered. Similar arguments were used previously (13) to show that no disordered solvent was present in the RNase S mutants at position 13. Such arguments can also be used to rule out disordered water in the human lysozyme mutants which have relatively small cavities. The only mutants in which there may be disordered water are the L133A, F153A, and L99A mutants of T4 lysozyme and L14A, I88A, and I96A mutants of barnase. The presence of disordered water in favorable cases can be detected from

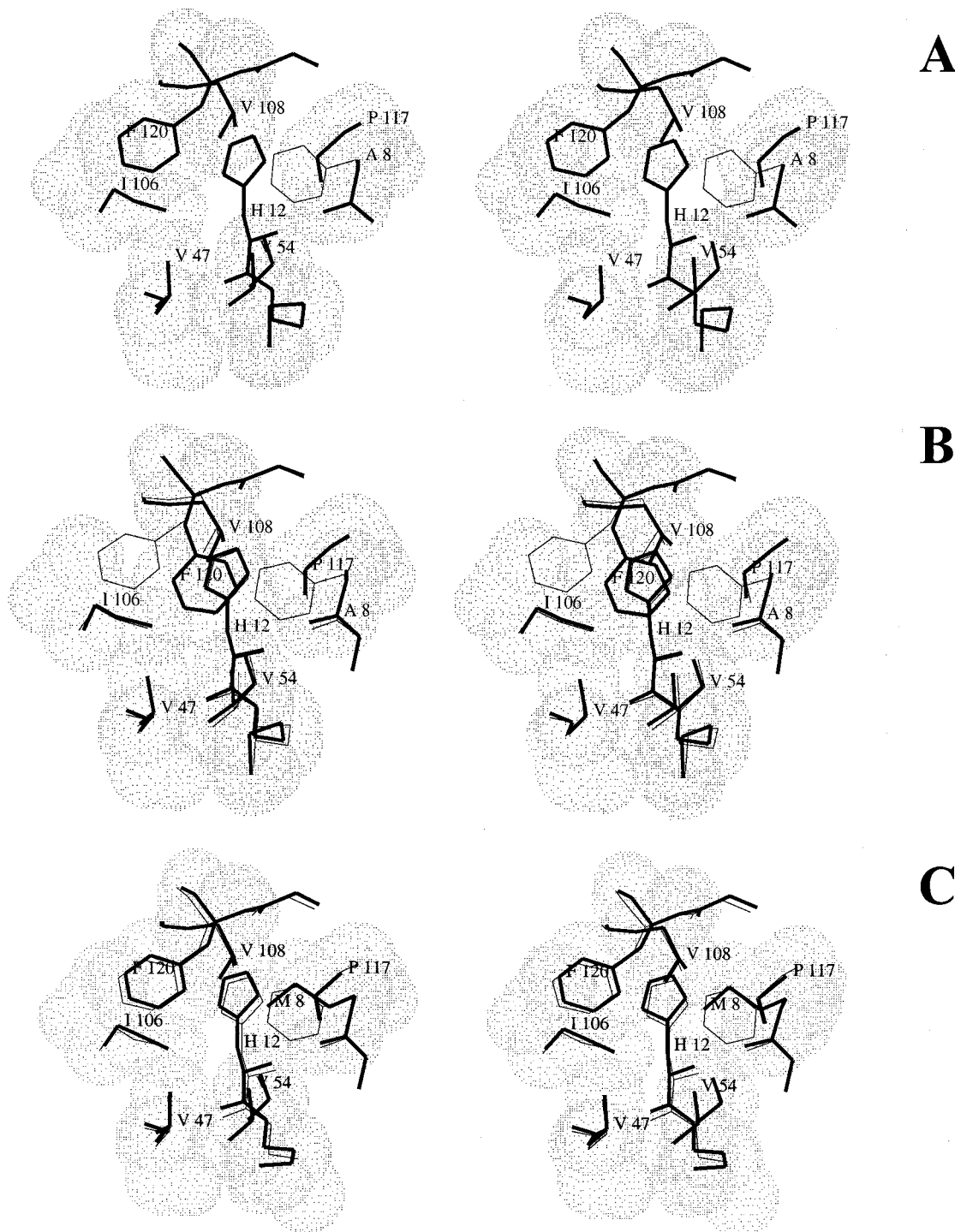


FIGURE 1: Stereoplots of the F8X structures (thick line) superimposed on their respective controls (thin line) in the region around residue 8. A single cavity is present in each structure. The van der Waals dot surface of residues around the cavity is shown for the F8X structures to highlight the cavity that is formed. The dot surface for residue H12 has not been displayed in all the figures. (A) Model of the F8A mutant with all the atoms beyond the  $C_{\beta}$  of residue 8 deleted, superimposed on the control indicating the potential cavity. (B) The actual structure of the F8A mutant showing the movement of the F120 side chain, which minimizes the potential cavity. (C) The structure of the F8M superimposed on its control. The structure of F8Nle is virtually similar to F8M in terms of overall structure and also the side chain conformation of residue 8.

analysis of low-resolution reflections (38). However, as discussed below, even if disordered water were present in a few of the cavity-containing mutants, it would not significantly alter the main conclusions of this study.

*Thermodynamics of Binding of F8X Peptides to the S Protein.* The binding of the various F8X peptides and deletion peptides to the S protein was measured under conditions [100 mM NaCl and 50 mM sodium acetate (pH

6.0)] identical to those of the M13X peptides (20–22). The F8M and F8Nle peptide bound tightly to the S protein, and the binding constant ( $K$ ) and the  $\Delta H^{\circ}$  could be determined accurately over the temperature range of 6–25 °C (Supporting Information). The binding of the F8M peptide is weaker than that of F8Nle at all temperatures by 0.5–1.0 kcal mol<sup>-1</sup>. The binding of the F8A peptide to the S protein could not be determined under these conditions. Binding could only

Table 2: Difference Thermodynamic Parameters for Peptide Binding to the S Protein at 25 °C

peptide <sup>a</sup>	$\Delta\Delta H^\circ(25\text{ }^\circ\text{C})$ (kcal mol <sup>-1</sup> )	$\Delta\Delta C_p$ (K <sup>-1</sup> )	$\Delta\Delta G^\circ(25\text{ }^\circ\text{C})$ (kcal mol <sup>-1</sup> )	$T\Delta\Delta S^\circ(25\text{ }^\circ\text{C})$ (kcal mol <sup>-1</sup> )
Nle13I	-2.5	0.02	-0.7	-1.8
Nle13L	-2.2	-0.09	-0.5	-1.9
<b>I13V</b>	<b>-1.9</b>	<b>-0.04</b>	<b>-0.2</b>	<b>-1.7</b>
Nle13M	-7.9	-0.19	-0.8	-7.1
<b>Nle13A</b>	<b>-5.1</b>	<b>-0.39</b>	<b>3.5</b>	<b>-8.6</b>
<b>Nle13ANB</b>	<b>1.3</b>	<b>-0.02</b>	<b>0.7</b>	<b>0.6</b>
<b>F8M</b>	<b>14.7</b>	<b>0.39</b>	<b>3.6</b>	<b>11.1</b>
<b>F8Nle</b>	<b>10.0</b>	<b>0.0</b>	<b>2.9</b>	<b>7.1</b>
<b>F8A</b>	<b>17.7</b>	—	<b>5.1</b>	<b>12.6</b>
S(4-14)	0	—	1.5	-1.5
S(8-14)	4.0	—	2.5	1.5

<sup>a</sup> Thermodynamic parameters for the M13X mutants from ref 20. Titration data for the F8X mutants, controls, and deletion peptides are tabulated as Supporting Information. The large to small mutations are highlighted in bold.

be detected in the presence of phosphate [100 mM NaCl and 50 mM phosphate (pH 7.0)] at <15 °C. The  $\Delta H^\circ_{\text{obs}}$  and the  $\Delta G^\circ_{\text{obs}}$  were fit to estimate the  $\Delta C_p$ ,  $\Delta H^\circ(25\text{ }^\circ\text{C})$ , and  $\Delta G^\circ(25\text{ }^\circ\text{C})$  as described previously (20–22). These values are tabulated as Supporting Information. Values of  $\Delta C_p$  for the F8M and F8Nle peptides differ significantly from each other. Conservative substitutions of the Met sulfur atom with a methylene group are accompanied by unexpectedly large values of  $\Delta\Delta H^\circ$  and  $\Delta\Delta S$  (20). To interpret the thermodynamic data for large to small residue replacements without these complications, all the M13X thermodynamic and structural data were recalculated for a Nle13X or I13X mutant using the data in Table 2 of ref 20. Differences in thermodynamic parameters at 25 °C are summarized in Table 2. The data for the large to small mutants are highlighted in bold. The difference parameters indicate that the  $\Delta\Delta H^\circ$  for the F8X mutants is the highest of all the mutants with the F8M and F8A mutation causing a loss of almost 50% of the binding enthalpy associated with the S peptide–S protein interaction (Table 2). In comparison, the deletion of four residues (S4–14) and eight residues (S8–14) of S15 causes losses of only 0 and 10%, respectively, of the total binding enthalpy of the S15 peptide. The F8M and F8Nle complex exhibits activity similar to that of RNase S, whereas the F8A complex exhibits no detectable activity at pH 7.1.

The F8M and F8Nle structures are practically identical. However, there are decreases in  $\Delta H^\circ$ ,  $\Delta S$ , and  $\Delta C_p$  of binding and a stabilization of the F8Nle complex by 0.7 kcal mol<sup>-1</sup> relative to F8M at 25 °C. The signs of the changes in all four thermodynamic parameters (Table 2) are opposite of those observed for the M13Nle substitution (20). These results indicate while replacement of Met with Nle is isosteric, the thermodynamic consequences are strongly and surprisingly position-dependent and not determined solely by the hydrophobic effect.

**Correlation of Thermodynamic Parameters with Structure.** The thermodynamic parameters ( $\Delta\Delta G^\circ_{\text{obs}}$ ,  $\Delta\Delta G^\circ_{\text{corr}}$ , and  $\Delta\Delta H^\circ$ ) determined for the S peptide–S protein interaction were correlated with structural parameters (cavity volume, depth, OS, and  $\Delta\Delta\text{ASA}$ ) calculated from the crystal structures of the RNase S mutants. In the case of cavity-creating mutants of T4 lysozyme, it has been shown (30) that  $\Delta\Delta G^\circ_{\text{corr}}$  ( $\Delta\Delta G^\circ_{\text{obs}} - \Delta\Delta G^\circ_{\text{tr}}$ ) correlates better with changes

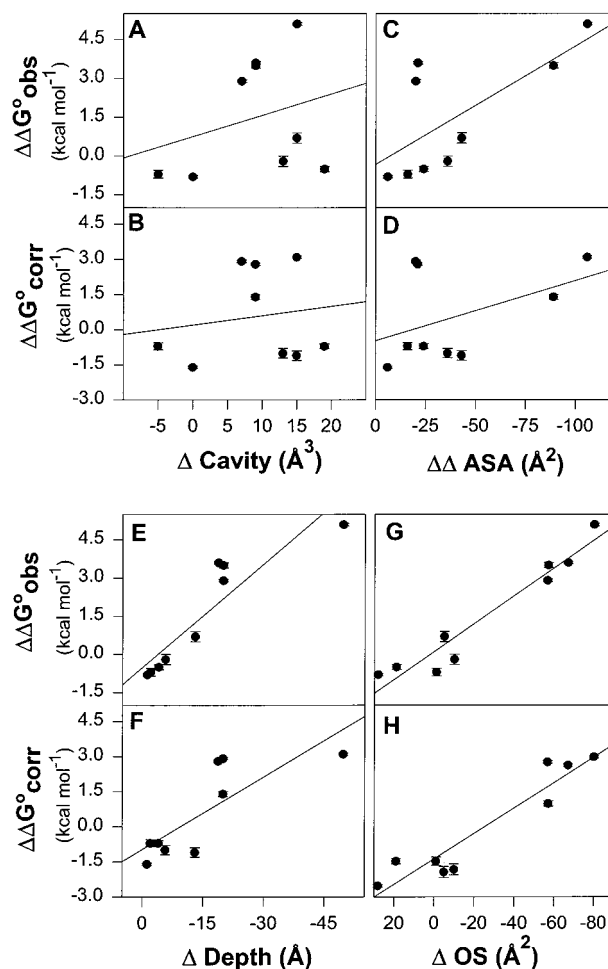


FIGURE 2: Correlation of  $\Delta\Delta G^\circ$  for mutants of RNase S (at residue 8 or 13) with structural parameters. The correlation statistics are listed in Table 3.  $\Delta\Delta G^\circ_{\text{corr}} = \Delta\Delta G^\circ_{\text{obs}} - \Delta\Delta G^\circ_{\text{tr}}$ .

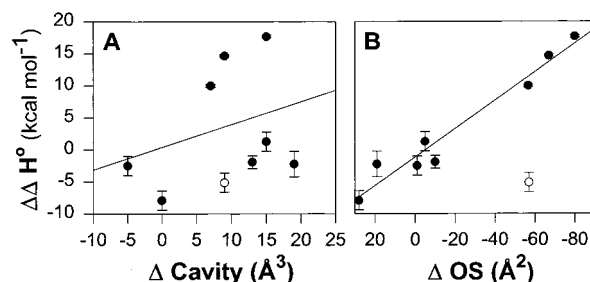


FIGURE 3: Correlation of  $\Delta\Delta H^\circ$  for mutants of RNase S (at residue 8 or 13) with structural parameters. The correlation statistics are listed in Table 3. The M13A structure (○) has a water molecule inside the cavity created and is not used in the correlation calculations.

in cavity volume than  $\Delta\Delta G^\circ_{\text{obs}}$ . However, for the RNase S mutants examined here, the correlation of  $\Delta\Delta G^\circ_{\text{corr}}$  with structural parameters was generally poorer than corresponding correlations using  $\Delta\Delta G^\circ_{\text{obs}}$  (Figure 2). The slope and the intercept for the plot of  $\Delta\Delta G^\circ_{\text{corr}}$  versus  $\Delta\text{Cavity}$  is different for RNase S (Table 3) than that observed previously for T4 lysozyme (12, 30). The best correlation of  $\Delta\Delta G^\circ_{\text{obs}}$  was with  $\Delta\text{Depth}$  and  $\Delta\text{OS}$ . The correlation of  $\Delta\Delta H^\circ$  with structural parameters (Figure 3) showed that  $\Delta\Delta H^\circ$  correlated best with  $\Delta\text{OS}$  and not with  $\Delta\text{Cavity}$ . The M13A structure had a water molecule in the cavity and was not included in the correlation. The errors for the thermodynamic parameters

Table 3: Slopes, Y-Intercepts, and Correlation Coefficients for the Correlation of Structural and Thermodynamic Data of Cavity-Containing Mutants<sup>a</sup>

Y	X <sup>b</sup>	Y-intercept (kcal mol <sup>-1</sup> )	slope <sup>c</sup>	correlation coefficient
T4 lysozyme				
$\Delta\Delta G^{\circ}_{\text{obs}}$	$\Delta\text{Cavity}(p)$	2.0	0.02	0.78
$\Delta\Delta G^{\circ}_{\text{corr}}$	$\Delta\text{Cavity}(p)$	0.42	0.018	0.87
$\Delta\Delta H^{\circ}$	$\Delta\text{OS}$	10.2	-0.38	0.72
Figure 2				
(A) $\Delta\Delta G^{\circ}_{\text{obs}}$	$\Delta\text{Cavity}(p)$	0.75	0.08	0.26
(B) $\Delta\Delta G^{\circ}_{\text{corr}}$	$\Delta\text{Cavity}(p)$	0.20	0.04	0.15
(C) $\Delta\Delta G^{\circ}_{\text{obs}}$	$\Delta\Delta\text{ASA}$	-0.31	-0.04	0.67
(D) $\Delta\Delta G^{\circ}_{\text{corr}}$	$\Delta\Delta\text{ASA}$	-0.45	-0.02	0.38
(E) $\Delta\Delta G^{\circ}_{\text{obs}}$	$\Delta\text{Depth}$	-0.50	-0.13	0.90
(F) $\Delta\Delta G^{\circ}_{\text{corr}}$	$\Delta\text{Depth}$	-0.97	-0.10	0.80
(G) $\Delta\Delta G^{\circ}_{\text{obs}}$	$\Delta\text{OS}$	0.11	-0.05	0.95
(H) $\Delta\Delta G^{\circ}_{\text{corr}}$	$\Delta\text{OS}$	-0.61	-0.05	0.94
Figure 3				
(A) $\Delta\Delta H^{\circ}$	$\Delta\text{Cavity}$	0.40	0.35	0.30
(B) $\Delta\Delta H^{\circ}$	$\Delta\text{OS}$	-1.14	-0.22	0.98
$\Delta\Delta H^{\circ}$	$\Delta\Delta\text{ASA}$	-2.0	-0.15	0.59
$\Delta\Delta H^{\circ}$	$\Delta\text{Depth}$	-3.6	-0.48	0.89
Figure 4				
(A) $\Delta\Delta G^{\circ}_{\text{obs}}$	$\Delta\text{Cavity}(p)$	0.97	0.034	0.64
(B) $\Delta\Delta G^{\circ}_{\text{corr}}$	$\Delta\text{Cavity}(p)$	-0.15	0.024	0.57
$\Delta\Delta G^{\circ}_{\text{obs}}$	$\Delta\text{Cavity}(c)$	1.32	0.031	0.60
$\Delta\Delta G^{\circ}_{\text{corr}}$	$\Delta\text{Cavity}(c)$	0.1	0.022	0.53
(C) $\Delta\Delta G^{\circ}_{\text{obs}}$	$\Delta\text{Depth}$	-0.34	-0.13	0.86
(D) $\Delta\Delta G^{\circ}_{\text{corr}}$	$\Delta\text{Depth}$	-0.16	-0.09	0.74
$\Delta\Delta G^{\circ}_{\text{obs}}$	$\Delta\text{OS}$	-0.04	-0.05	0.78
$\Delta\Delta G^{\circ}_{\text{corr}}$	$\Delta\text{OS}$	-0.90	-0.03	0.70
$\Delta\Delta G^{\circ}_{\text{obs}}$	$\Delta\Delta\text{ASA}$	-0.34	-0.04	0.75
Figure 5				
(A) $\Delta\Delta H^{\circ}$	$\Delta\text{Cavity}$	4.16	0.12	0.42
(B) $\Delta\Delta H^{\circ}$	$\Delta\text{OS}$	-1.85	-0.25	0.86
$\Delta\Delta H^{\circ}$	$\Delta\text{Depth}$	-2.4	-0.56	0.78
$\Delta\Delta H^{\circ}$	$\Delta\Delta\text{ASA}$	-5.3	-0.38	0.65

<sup>a</sup> Data for T4 lysozyme and for correlations not shown in the figures are also listed. <sup>b</sup> Published (p) and calculated (c) cavity volumes. <sup>c</sup> Units for slope: kcal mol<sup>-1</sup> Å<sup>-3</sup> for cavity volumes, kcal mol<sup>-1</sup> Å<sup>-1</sup> for depth, and kcal mol<sup>-1</sup> Å<sup>-2</sup> for OS and ASA.

utilized in our study are from refs 20–22, and these are shown in the figures as error bars.

In previous mutational studies, changes in thermodynamic parameters were correlated with structural parameters for the particular protein that was being studied. However, this makes it difficult to assess the generality of the observed correlations. We have therefore examined the correlations of thermodynamics with structural parameters for a larger data set of 41 cavity-containing mutants in four proteins (see Materials and Methods). In the data set, values of  $\Delta\text{Cavity}$  range from -5 to 153 Å<sup>3</sup> and values of  $\Delta\Delta G^{\circ}_{\text{obs}}$  range from -0.5 to 5.1 kcal mol<sup>-1</sup>. Figure 4 shows that  $\Delta\Delta G^{\circ}_{\text{obs}}$  correlates better (Table 3) with the structural parameters than does  $\Delta\Delta G^{\circ}_{\text{corr}}$ . This underscores the difficulty of applying corrections derived from small molecule free energy of transfer experiments to protein unfolding data. It also suggests that these corrections do not properly describe hydration contributions to the observed thermodynamics. It is worth noting that the  $\Delta\Delta G^{\circ}_{\text{tr}}$  data are measured at 25 °C, whereas in many studies, the  $\Delta\Delta G^{\circ}_{\text{obs}}$  and  $\Delta\Delta H^{\circ}_{\text{obs}}$  values are measured at higher temperatures or in the presence of denaturant.  $\Delta\Delta G^{\circ}_{\text{obs}}$  correlates best with  $\Delta\text{Depth}$  ( $r = 0.86$ ) and significantly worse with  $\Delta\text{Cavity}$  ( $r = 0.64$ ). This is probably because reliable estimation of cavity volumes in proteins is difficult and different methods can give quite

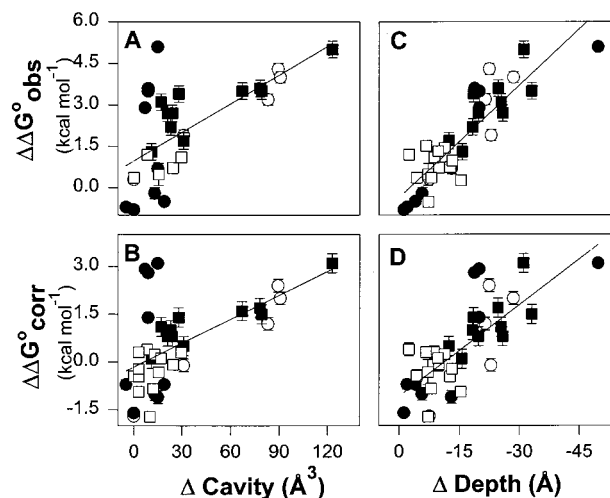


FIGURE 4: Correlation plots for  $\Delta\Delta G^{\circ}$  with structural parameters for cavity-containing mutants of RNase S (●), T4 lysozyme (■), human lysozyme (□), and barnase (○). The correlation statistics are listed in Table 3.

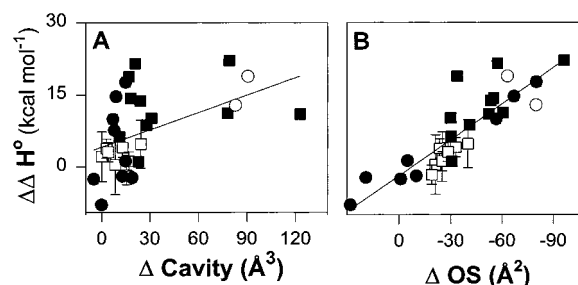


FIGURE 5: Correlation plots for  $\Delta\Delta H^{\circ}$  with structural parameters for cavity-containing mutants of RNase S (●), T4 lysozyme (■), human lysozyme (□), and barnase (○). The correlation statistics are listed in Table 3.

different estimates (39). For the correlation's estimate, we used cavity volumes published in the literature as well as cavity volumes recalculated for all the structures using a 1.2 Å probe and the MSP procedure (25). The correlations are better for the published values than for the calculated values in each case.

A unique feature of the RNase S system is that accurate estimates of  $\Delta\Delta H^{\circ}(25\text{ °C})$  can also be obtained without extrapolation. In the past, it has been difficult to correlate values of  $\Delta\Delta H^{\circ}$  with structural parameters (12, 13, 30–32). In the case presented here,  $\Delta\Delta H^{\circ}(25\text{ °C})$  correlates well ( $r = 0.98$ ; Figure 3B and Table 3) with  $\Delta\text{OS}$ , with the exception of one mutant, M13A, which has a low binding enthalpy because of the presence of an ordered water molecule in the cavity. The  $\Delta\Delta H^{\circ}$  values for mutants of T4 lysozyme and human lysozyme also correlate well with  $\Delta\text{OS}$  (Figure 5 and Table 3). A fit using the data for all four proteins shows a high correlation coefficient of 0.86. The errors for the thermodynamic parameters utilized in Figures 4 and 5 are from refs 12, 13, 20–22, 30–32, and 35, and these are shown as error bars. The errors for the  $\Delta H^{\circ}$  values are not available for mutants of T4 lysozyme and barnase utilized in our study.

The fitted slopes for RNase S ( $-0.22\text{ kcal mol}^{-1}\text{ Å}^{-2}$ ) also compare well with that for all four proteins ( $-0.25\text{ kcal mol}^{-1}\text{ Å}^{-2}$ ). It should be emphasized that this result is the first clear correlation of  $\Delta\Delta H^{\circ}$  with structural parameters.

Table 4: Differences in Thermodynamic Parameters for Transfer ( $\Delta\Delta X_{tr}$ ) for Some Typical Nonpolar Substances from Water to an Organic Solvent at 25 °C<sup>a</sup>

	$\Delta\Delta G^\circ$ (kcal mol <sup>-1</sup> )	$\Delta\Delta H^\circ$ (kcal mol <sup>-1</sup> )	$T\Delta\Delta S$ (kcal mol <sup>-1</sup> )	$\Delta\Delta S$ (cal mol <sup>-1</sup> K <sup>-1</sup> )	ref
water → liquid phase					
toulene → benzene	0.8	-0.08	-0.88	-2.95	5
ethylbenzene → benzene	1.6	-0.01	-1.61	-5.39	5
hexane → pentane	0.95	0.5	-0.45	-1.50	5
water → <i>n</i> -hexanol					
Val → Ala	1.08	0.5	-0.58	-1.94	37
Leu → Ala	1.68	0.3	-1.38	-4.62	37
Nle → Ala	1.90	0.1	-1.80	-6.03	37
mutation <sup>b</sup>					
Val → Ala	1.2 ± 0.6 (9)	3.9 ± 3 (9)	2.7	9.05	30, 32
Leu → Ala	3.6 ± 0.8 (7)	13.1 ± 5 (5)	9.5	31.8	30, 33
Ile → Ala	3.0 ± 0.7 (5)	16.0 ± 3 (4)	13.0	43.6	30, 33
Phe → Ala	4.3 ± 1 (2)	20.0 ± 3 (2)	15.7	52.6	20, 30

<sup>a</sup> These values are compared to changes in folding thermodynamics upon mutation in proteins ( $\Delta X_{mutant} - \Delta X_{wild\ type}$ ). <sup>b</sup> The thermodynamic parameters ( $\Delta\Delta X$ ) listed in the mutation section are average values of a number (in parentheses) of mutants.

The occluded surface appears to be a convenient geometric measure of the extent of van der Waals interactions between residues, and it will be of interest to see how well these correlations hold in future studies.

## DISCUSSION

While naturally occurring proteins are well-packed, the role of packing interactions in determining the fold remains controversial. While it has been suggested that the basic globular fold may be specified by hydrophobic interactions rather than packing (40), mutations of large bulky side chains to those which occupy smaller volumes (12, 13) are accompanied by large changes in enthalpy and invariably destabilize the folded state of the protein. This occurs both because of cavity formation and consequent loss of van der Waals interactions and through a decrease in the hydrophobic driving force for folding (3, 4). In studies of T4 lysozyme, the contribution of packing was estimated to be 0.022 kcal mol<sup>-1</sup> Å<sup>-3</sup> of cavity volume, while the hydrophobic effect contribution was estimated from water to octanol (36) free energies of transfer. However, our work shows that cavity volume is poorly correlated with values of  $\Delta\Delta G^\circ_{corr}$  in other systems, and hence, this approach cannot be generalized. This is probably due to the lack of a reliable procedure for accurate estimation of cavity volumes. We have previously shown that changes in residue depth correlate very well with values of  $\Delta\Delta G^\circ$  for large to small substitutions in several proteins (27). This correlation also holds good for the data set of cavity-containing mutants examined in this work.

The depth of a residue is a measure of its distance from the protein surface. The better correlation of  $\Delta\Delta G^\circ$  with depth than with  $\Delta\Delta ASA$  probably results from the fact that the protein interior has significantly higher packing density than the bulk solvent (41). Consequently, the strengths of van der Waals interactions in the protein interior are likely to be higher than in bulk solvent or close to the protein surface.

$\Delta C_p$  is an important thermodynamic parameter that determines the temperature dependence of  $\Delta H^\circ$ ,  $\Delta S$ , and  $\Delta G^\circ$ . For RNase S (Table 2), large to small substitutions typically do not affect  $\Delta C_p$ . The average  $\Delta\Delta C_p$  change is  $-0.02 \pm 0.04$  kcal mol<sup>-1</sup> K<sup>-1</sup>. This does not include the substitutions involving Met and the structure containing

ordered water. Results from DSC studies of human lysozyme (average  $\Delta\Delta C_p = 0.13 \pm 0.23$  kcal mol<sup>-1</sup> K<sup>-1</sup>) also confirm this assertion (31, 32). This is an important result because it suggests that values of  $\Delta\Delta H^\circ$  and  $\Delta\Delta S$  that result from large to small substitutions are relatively independent of temperature. The only exceptions occur when bound water is found in the cavity or when there is a change in atom type such as in the Met → Nle or Phe → Met substitution. Met to Nle substitutions have surprisingly large and position-dependent changes in  $\Delta C_p$ . The changes are much larger than predicted from small molecule experiments (42).

The hydrophobic effect is typically quantitated in terms of the thermodynamics of transfer of nonpolar molecules from water to organic solvents. At room temperature for such transfer processes, values of  $\Delta H^\circ_{tr}$  are close to zero while values of  $\Delta S_{tr}$  are positive. With a decrease in the size of the solute, values of  $\Delta\Delta H^\circ_{tr}$  are generally close to zero. Since the sign of  $\Delta\Delta H^\circ_{tr}$  depends on differences between small numbers, the sign can be either positive or negative. However, values of  $\Delta\Delta S_{tr}$  are always large and negative, and result in a positive value of  $\Delta\Delta G^\circ_{tr}$  (Table 4) for a small nonpolar solute with respect to a larger one (3). These negative values of  $\Delta\Delta S_{tr}$  are considered the hallmark of the hydrophobic effect. The mutational data for RNase S in Table 2 (in bold) show that substitutions of large nonpolar amino acids with smaller ones typically result in large positive values of  $\Delta\Delta H^\circ$  and  $\Delta\Delta S$ . The only exceptions to this are the I13V and Nle13A substitutions. In the former case, the magnitudes of  $\Delta\Delta H^\circ$  and  $\Delta\Delta S$  are small, consistent with the conservative nature of the substitution. There is a small stabilization upon mutation, suggesting that some steric strain in the complex has been removed upon mutation. In the latter case, the presence of a bound water molecule in a cavity present in the crystal structure of the A13 mutant is the probable cause of the negative values of  $\Delta\Delta H^\circ$  and  $\Delta\Delta S$ . In all other cases, for large to small mutations, enthalpic effects are dominant and result in a positive value of  $\Delta\Delta G^\circ$ . Identical trends in  $\Delta\Delta H^\circ$  and  $\Delta\Delta S$  are observed for large to small substitutions in T4 lysozyme, human lysozyme, and barnase (Figure 5; 25, 30, 31, 35). Although these studies were carried out at higher temperatures, the observation that  $\Delta\Delta C_p$  is close to zero for such substitutions means that values of  $\Delta\Delta H^\circ$  and  $\Delta\Delta S$  for all these proteins are temperature-

independent. The sign of  $\Delta\Delta S$  is consistently the reverse of that expected from the hydrophobic effect (Tables 2 and 4). Furthermore, the positive values of  $\Delta\Delta G^\circ$  are primarily due to large, positive values of  $\Delta\Delta H^\circ$ . In contrast, in the case of transfer thermodynamic data, positive values of  $\Delta\Delta G^\circ_{tr}$  are always associated with negative values of  $\Delta\Delta S_{tr}$  (Table 4). The temperature independence of  $\Delta\Delta H^\circ$  and  $\Delta\Delta S$  and the observation that enthalpic effects are dominant suggest that the hydrophobic effect is not an important contributor to the observed energetics. Hydration effects are strongly temperature-dependent (43) in contrast to the observed thermodynamics. Another factor which suggests that hydrophobic effects are not dominant is the fact that observed values of  $\Delta\Delta G^\circ$  correlate better with  $\Delta\text{Depth}$  than with  $\Delta\Delta\text{ASA}$  (Figure 2 of ref 27). The hydrophobic effect results largely from unfavorable interactions of nonpolar groups in water. If the hydrophobic effect were dominant, then two identical nonpolar residues with similar accessibility but different depths would contribute equally to protein stabilization. This is clearly not the case. The positive sign of  $\Delta\Delta H^\circ$  suggests that the loss of packing interactions rather than the hydrophobic effect makes the largest energetic contribution. Values of  $\Delta\Delta H^\circ$  for cavity-containing mutants of different proteins measured at different temperatures correlate best with  $\Delta\text{OS}$  (Figures 3 and 5 and Table 3). This is again consistent with packing interactions contributing significantly to  $\Delta\Delta H^\circ$ . The few mutants with negative values of  $\Delta\Delta H^\circ$  all have negative values of  $\Delta\Delta G^\circ$ , suggesting that removal of unfavorable steric interactions has resulted in stabilization of the protein. Most cavity-creating substitutions are associated with positive  $\Delta\Delta S$  values.

Entropy–enthalpy compensation is believed to be a general feature of weak interactions (44). In many cases, this is taken to be an indication of involvement of solvent or solvation changes in the process. However, in our case this is unlikely. The crystal structures do not show any evidence of solvation changes in the folded state. In any case, for the kind of nonpolar substitutions involved, no such changes (with the exception of cavity-filling waters) are expected. CD spectroscopy has previously been used to show that in the RNase S system, at room temperature, the peptide is largely in a random coil state before binding and that the substitutions have negligible effects on the structure of the free peptide (the unfolded state). All the peptides used in this study are all random coils in the free state (data not shown). Any solvation changes in the free peptide that result from amino acid substitutions in the free peptide are precisely those that contribute to the hydrophobic effect. As discussed above, if these solvation changes were important contributors to the observed thermodynamics, then large to small substitutions would be accompanied by *negative* values of  $\Delta\Delta S$  and smaller (in magnitude) values of  $\Delta\Delta H^\circ$ . This is not what is observed. Hence, the observed entropy–enthalpy compensation is unlikely to be due to changes in solvent structure in the folded state or the hydrophobic effect. The positive values of  $\Delta\Delta S$  are probably due to an increase in entropy of the folded state in cavity-creating mutants. This increased entropy is predicted from simple packing calculations in model systems (14). However, there are as yet no systematic, quantitative computational studies that rationalize the measured values of  $\Delta\Delta S$  for the cavity-containing mutants mentioned in this study.

There appear to be only a few possible explanations for the observed thermodynamics for large to small substitutions. (a) Entropic and enthalpic changes, even for such a relatively simple binding reaction, are uninterpretable. If this is indeed the case, this would render invalid most published calorimetric data on protein folding thermodynamics. (b) The observed changes are indeed due to the hydrophobic effect. While transfer of nonpolar groups from water to organic solvent occurs with either positive or negative enthalpy changes (3, 45), invariably such transfer processes are accompanied by a positive entropy change. It is hard to reconcile the large positive values of  $\Delta\Delta S$  seen in mutational studies (Table 4) with results from transfer studies. The positive values of  $\Delta\Delta S$  are unlikely to result from conformational entropy effects for two reasons. First, they are much larger than estimates of changes in conformational entropy from a variety of theoretical and experimental studies (46). Second, even in cases where the smaller side chain has more conformational degrees of freedom than the larger one (e.g., F8Nle), positive values of  $\Delta\Delta S$  are still observed. The positive values of  $\Delta\Delta S$  are unlikely to be due to the presence of disordered water molecules in any of the cavity-containing mutants for two reasons. First, most of the cavities are too small to contain disordered water. Second, transfer of water from bulk solvent to the protein interior would be associated with a negative rather than a positive value of  $\Delta\Delta S$ . (c) The explanation that we favor is that the observed thermodynamics are primarily due to the loss of packing interactions in the folded state of cavity-containing mutants. This result is also in agreement with recent computational studies (47, 48).

For many years, the hydrophobic effect has been thought to be one of the dominant driving forces in protein folding. Most of the evidence for this is based on the thermodynamics of transfer of small molecules from water to another reference phase. A major complication with such studies is that there is no solvent–solid reference phase that is a sufficiently good mimic of protein interiors, although a variety of organic solvents, amino acid crystals, and the gas phase have been used. A recent analysis (43) using a variety of transfer thermodynamic data suggested that close packing rather than hydration effects is the dominant contribution of nonpolar groups to protein stability. The work presented here suggests that the loss of packing interactions in the folded state, rather than the hydration effects, is responsible for the decreased stability of cavity-creating mutants. Previous studies (15) have associated values of  $\Delta\Delta G^\circ$  from such studies with the hydrophobic driving force. The work presented here clearly indicates that there are serious problems with such an approach. The observed values of  $\Delta\Delta G^\circ$  contain contributions from loss of packing interactions as well as the hydrophobic effect. Recent studies of T4 lysozyme mutants (12, 30) have attempted to take into account the packing contribution by measuring cavity volumes. However, as seen here, cavity volumes are difficult to calculate and correlations of observed values of  $\Delta\Delta G^\circ$  with cavity volume are poor. If one accepts the suggestion that the observed thermodynamics in cavity-creating mutants are dominated by packing effects, then current magnitudes of the hydrophobic effect [20–50 cal mol<sup>-1</sup> Å<sup>-2</sup> (15, 30, 39)] are likely to be overestimates. This is entirely in agreement with the suggestion of Makhatadze and Privalov (43) that was developed by very different means.

The dominant role of packing may also explain the puzzling observation that proteins are denatured by high pressures whereas the hydrophobic driving force as measured in transfer experiments increases with increased pressure (2). Hummer et al. (49) offer an explanation in which pressure destabilization of hydrophobic aggregates and the penetration of water inside the hydrophobic core explain the denaturation of proteins. This discrepancy could also be due to the differences in compressibility between proteins and the organic and aqueous solvents used in the transfer experiments. Closely packed, folded proteins have much lower compressibilities (50) than aqueous or organic solvents. Consequently, at increased pressures, there is likely to be little change in van der Waals interactions in the folded protein, but a significant increase in the strength of van der Waals interactions between the protein and solvent in the denatured state is likely. This results in a more positive value of  $\Delta G^\circ_f$  at high pressure. In the case of transfer measurements, since organic solvents are more compressible than water (51), increased pressures would result in a greater increase in the strength of van der Waals interactions in the organic than in the aqueous phase. Hence, the value of  $\Delta G^\circ_{tr}$  would become more negative with increasing pressure.

Most of the evidence for the magnitude of hydrophobic stabilization in protein folding comes from small molecule transfer data. There are significant differences between transfer thermodynamics and protein folding. It is now relatively straightforward to mutate proteins and characterize folding thermodynamics through calorimetry. However, the number of protein systems for which detailed mutational, structural, and thermodynamic data are all available is still small. There have also been several improvements in computational methods for studying protein folding thermodynamics (52). A combined use of experimental and computational approaches, rather than reliance on small molecule transfer data, should greatly facilitate quantitative understanding of folding energetics.

## ACKNOWLEDGMENT

Computational facilities of the Supercomputer Education Research Center and the Interactive Graphics facility have been utilized for this work. The X-ray data were collected at the Image Plate Facility at the Molecular Biophysics Unit (MBU). This work has been done in part in MBU while G.S.R. was a graduate student and also in the National Centre for Biological Sciences (NCBS) where G.S.R. is a postdoctoral visiting fellow. We thank Prof. Jayant Udgaonkar (NCBS) for use of the titration calorimeter and S. Chakravarty for helpful discussions.

## SUPPORTING INFORMATION AVAILABLE

Tables with titration calorimetric data for RNase S mutants (6–25 °C) and their controls (25 °C). This material is available free of charge via the Internet at <http://pubs.acs.org>.

## REFERENCES

1. Kauzmann, W. (1959) *Adv. Protein Chem.* 11, 14–63.
2. Kauzmann, W. (1987) *Nature* 325, 763–764.
3. Privalov, P. L., and Gill, S. J. (1988) *Adv. Protein Chem.* 39, 191–234.
4. Dill, K. A. (1990) *Biochemistry* 29, 7133–7151.

5. Privalov, P. L., and Gill, S. J. (1989) *Pure Appl. Chem.* 61, 1097–1104.
6. Baldwin, R. L. (1986) *Proc. Natl. Acad. Sci. U.S.A.* 83, 8069–8072.
7. Murphy, K. P., Privalov, P. L., and Gill, S. J. (1990) *Science* 247, 559–560.
8. Pace, C. N. (1992) *J. Mol. Biol.* 226, 29–35.
9. Sturtevant, J. (1994) *Curr. Opin. Struct. Biol.* 4, 69–78.
10. Matthews, B. W. (1995) *Adv. Protein Chem.* 46, 249–278.
11. Varadarajan, R., Richards, F. M., and Connelly, P. R. (1990) *Curr. Sci.* 59, 819–824.
12. Eriksson, A. E., Baase, W. A., Zhang, X. J., Heinz, D. W., Blaber, M., Baldwin, E. P., and Matthews, B. W. (1992) *Science* 255, 178–183.
13. Varadarajan, R., and Richards, F. M. (1992) *Biochemistry* 31, 12313–12327.
14. Richards, F. M., and Lim, W. A. (1993) *Q. Rev. Biophys.* 26, 423–498.
15. Jackson, S. E., Moracci, M., elMasry, N., Johnson, C. M., and Fersht, A. R. (1993) *Biochemistry* 32, 11259–11269.
16. Richards, F. M., and Vithyathil, P. J. (1959) *J. Biol. Chem.* 234, 1459–1465.
17. Richards, F. M., and Wyckoff, H. W. (1971) *Enzymes* 4, 647–806.
18. Kim, E. E., Varadarajan, R., Wyckoff, H. W., and Richards, F. M. (1992) *Biochemistry* 31, 12304–12314.
19. Goldberg, J. M., and Baldwin, R. L. (1999) *Proc. Natl. Acad. Sci. U.S.A.* 96, 2019–2024.
20. Thomson, J., Ratnaparkhi, G. S., Varadarajan, R., Sturtevant, J. M., and Richards, F. M. (1994) *Biochemistry* 33, 8587–8593.
21. Connelly, P. R., Varadarajan, R., Sturtevant, J. M., and Richards, F. M. (1990) *Biochemistry* 29, 6108–6114.
22. Varadarajan, R., Connelly, P. R., Sturtevant, J. M., and Richards, F. M. (1992) *Biochemistry* 31, 1421–1426.
23. Nadig, G., Ratnaparkhi, G. S., Varadarajan, R., and Vishveshvara, S. (1996) *Protein Sci.* 5, 2104–2114.
24. Ratnaparkhi, G. S., and Varadarajan, R. (1996) *Proteins* 36, 282–294.
25. Connolly, M. L. (1993) *J. Mol. Graphics* 11, 139–141.
26. Lee, B., and Richards, F. M. (1971) *J. Mol. Biol.* 55, 379–400.
27. Chakravarty, S., and Varadarajan, R. (1999) *Structure* 7, 723–732.
28. Pattabiraman, N., Ward, K. B., and Fleming, P. J. (1995) *J. Mol. Recognit.* 8, 334–344.
29. Kleywegt, G. J., and Jones, T. A. (1994) *Acta. Crystallogr. D50*, 178–185.
30. Xu, J., Baase, W. A., Baldwin, E. P., and Matthews, B. W. (1998) *Protein Sci.* 7, 158–177.
31. Takano, K., Ogasahara, K., Kaneda, H., Yamagata, Y., Fujii, S., Kanaya, E., Kikuchi, M., Oobatake, M., and Yutani, K. (1995) *J. Mol. Biol.* 254, 62–76.
32. Takano, K., Yamagata, Y., Fujii, S., and Yutani, K. (1997) *Biochemistry* 36, 688–698.
33. Buckle, A. M., Cramer, P., and Fersht, A. (1996) *Biochemistry* 35, 4298–4305.
34. Berstein, F. C., Koetzle, T. F., Williams, G. J. B., Meyer, E. F., Jr., Brice, M. D., Rodgers, J. R., Kennard, O., Shimanouchi, T., and Tasumi, M. (1977) *J. Mol. Biol.* 112, 535–542.
35. Pfeil, W. (1998) in *Protein Stability and Folding. A collection of thermodynamic data* (Pfeil, W., Ed.) Springer.
36. Fauchere, J. L., and Pliska, V. E. (1983) *Eur. J. Med. Chem.* 18, 369–375.
37. Nandi, P. K. (1976) *Int. J. Pept. Protein Res.* 8, 253–264.
38. Yu, B., Blaber, M., Gronenborn, A. M., Clore, G. M., and Caspar, D. L. D. (1999) *Proc. Natl. Acad. Sci. U.S.A.* 96, 103–108.
39. Vlasi, M., Cesareni, G., and Kokkinidid, M. (1999) *J. Mol. Biol.* 285, 817–827.
40. Behe, M. J., Lattman, E. E., and Rose, G. D. (1991) *Proc. Natl. Acad. Sci. U.S.A.* 88, 4195–4199.

41. Harpaz, Y., Gerstein, M., and Chothia, C. (1994) *Structure* 2, 641–649.
42. Spolar, R. S., Livingstone, J. R., and Record, M. T. (1992) *Biochemistry* 31, 3947–3955.
43. Makhatdze, G. I., and Privalov, P. L. (1995) *Adv. Protein Chem.* 47, 307–425.
44. Dunitz, J. D. (1995) *Chem. Biol.* 2, 709–712.
45. Blokzijl, W., and Engberts, J. B. F. N. (1993) *Angew. Chem., Int. Ed. Engl.* 32, 1545–1578.
46. Lee, K. H., Xie, D., Friere, E., and Amzel, M. (1994) *Proteins* 20, 68–84.
47. Kono, H., Saito, M., and Sarai, A. (2000) *Proteins* 38, 197–209.
48. Prevost, M., Wodak, S. J., Tidor, B., and Karplus, M. (1991) *Proc. Natl. Acad. Sci. U.S.A.* 88, 10880.
49. Hummer, G., Garde, S., Garcia, A. E., and Paulaitis, M. E. (1998) *Proc. Natl. Acad. Sci. U.S.A.* 95, 1552–1555.
50. Kundrot, C. E., and Richards, F. M. (1987) *J. Mol. Biol.* 193, 157–160.
51. Weast, R. C. (1975) in *CRC Handbook of Chemistry and Physics* (Weast, R. C., Ed.) CRC Press, Boca Raton, FL.
52. Lazaridis, T., Archontis, G., and Karplus, M. (1995) *Adv. Protein Chem.* 47, 231–306.

BI000775K